The American Journal of Pathology, Vol. 178, No. 6, June 2011

DOI: 10.1016/j.ajpath.2011.02.040

Cardiovascular, Pulmonary, and Renal Pathology

Length-Dependent Retention of Carbon Nanotubes in the Pleural Space of Mice Initiates Sustained Inflammation and Progressive Fibrosis on the Parietal Pleura

Fiona A. Murphy,* Craig A. Poland,*† Rodger Duffin,* Khuloud T. Al-Jamal,‡§ Hanene Ali-Boucetta,‡ Antonio Nunes,‡ Fiona Byrne,¶‖ Adriele Prina-Mello,¶‖ Yuri Volkov,¶‖ Shouping Li,** Stephen J. Mather,†† Alberto Bianco,‡‡ Maurizio Prato,** William MacNee,* William A. Wallace,§§¶¶ Kostas Kostarelos,‡ and Ken Donaldson*

From the University of Edinburgh/Medical Research Council, the Centre for Inflammation Research, Queen's Medical Research Institute, Edinburgh, United Kingdom; Safenano,† Institute of Occupational Medicine, Edinburgh, United Kingdom; the Nanomedicine Laboratory,‡ Centre for Drug Delivery Research, the School of Pharmacy, University of London, London, United Kingdom; the Department of Pharmacy,§ the Institute of Pharmaceutical Science, King's College London, London, United Kingdom; the School of Physics,¶ the Centre for Research on Adaptive Nanostructures and Nanodevices, and the School of Medicine,‖ Trinity College, Dublin, Ireland; the Department of Pharmaceutical Sciences,** Center of Excellence for Nanostructured Materials, University of Trieste, Trieste, Italy; the Department of Nuclear Medicine,†† St. Bartholomew's Hospital, London, United Kingdom; CNRS,‡‡ Institut de Biologie Moléculaire et Cellulaire, Immunologie et Chimie Thérapeutiques, Strasbourg, France; and the Department of Pathology,§§ Royal Infirmary of Edinburgh, and the Division of Pathology,¶¶ College of Medicine and Veterinary Medicine, University of Edinburgh, Edinburgh, United Kingdom*

The fibrous shape of carbon nanotubes (CNTs) raises concern that they may pose an asbestos-like inhalation hazard, leading to the development of diseases, especially mesothelioma. Direct instillation of long and short CNTs into the pleural cavity, the site of mesothelioma development, produced asbestos-like length-dependent responses. The response to long CNTs and long asbestos was characterized by acute inflammation, leading to progressive fibrosis on the parietal pleura, where stomata of strictly defined size limit the egress of long, but not short, fibers. This was confirmed by demonstrating clearance of short, but not long, CNT and nickel nanowires and by visualizing the migration of short CNTs from the pleural space by single-photon emission computed tomographic imaging. Our data confirm the hypothesis that, although a proportion of all deposited particles passes through the pleura, the pathogenicity of long CNTs and other fibers arises as a result of length-dependent retention at the stomata on the parietal pleura. ***(Am J Pathol 2011, 178:2587–2600; DOI: 10.1016/j.ajpath.2011.02.040)***

Carbon nanotubes (CNTs) are high-aspect ratio nanoparticles formed from a single graphene cylinder (single-walled CNTs) or several graphene cylinders stacked inside each other [multiwalled CNTs (MWCNTs)]. They are typically up to tens of nanometers in diameter but can

Supported in part by the Department of Health (F.A.M.); The Colt Foundation (C.A.P. and K.D.); the EC FP7 NAMDIATREAM (NMP-2009-246479) research project (F.B. and A.P.-M.) and Science Foundation Ireland, as part of the CRANN CSET-funded facilities; and the European Commission FP7 ANTICARB (HEALTH-2008-20157) research project (K.T.A.-J., A.B., M.P., and K.K.).

Accepted for publication February 9, 2011.

Author Contributions: F.A.M., C.A.P., R.D., and K.D. initiated, designed, and directed all experiments and took responsibility for planning and writing the manuscript; F.A.M., K.T.A.-J., A.N., and S.L. performed the SPECT/CT imaging experiment and analyzed the data; H.A.-B. performed transmission electron microscopy on the CNT panel; F.B., A.P.-M., and Y.V. manufactured and provided the NiNW samples and contributed to writing the manuscript; S.J.M. provided reagents and facilities for radiolabeling and SPECT/CT imaging; A.B., and M.P. prepared the short CNTs for labelling and analyzed the data; and S.L., A.B., W.M., and K.K. provided intellectual input and contributed to the writing of the manuscript.

This is an independent report commissioned and funded by the Policy Research Programme in the Department of Health. The views expressed are not necessarily those of the Department.

Address reprint request to Ken Donaldson, Ph.D., Centre for Inflammation Research, Queen's Medical Research Institute, 47 Little France Crescent, Edinburgh EH16 4TJ, United Kingdom. E-mail: ken.donaldson@ed.ac.uk.

Table 1. Characteristics of the carbon nanotube panel

Variable	NT_{short}	NT_{tang1}	NT_{tang2}	NT_{long1}	NT_{long2}	$NiNW_{short}$	$NiNW_{long}$
Source	Nanostructured & Amorphous Materials, Inc.	NanoLab, Inc.	NanoLab, Inc.	Mitsui & Co.	University of Manchester (Dr I. Kinloch)	CRANN–Trinity College Dublin (Drs F. Byrne and A. Prina-Mello)	CRANN–Trinity College Dublin (Drs F. Byrne and A. Prina-Mello)
Diameter (nm)							
Supplied by the manufacturer	20–30	15 ± 5	15 ± 5	40–50	20–100	4.3 ± 1.0	24.0 ± 7.0
Determined by the authors		14.84 ± 0.05	10.40 ± 0.32	84.89 ± 1.9	165.02 ± 4.68	200 ± 10	200 ± 10
Length as supplied by the manufacturer (μm)	0.5–2	1–5	5–20	13 (mean)	56 (maximum)	1–5	24 (median)
% of fibers							
>15 μm	ND	ND	ND	24.04	84.26	ND	85
>20 μm	ND	ND	ND	11.54	76.85	ND	73

Data are given as mean ± SEM.
CRANN, Centre for Research on Adaptive Nanostructures and Nanodevices; NiNW, nickel nanowires; ND, not detected.

extend to millimeters in length.[1] The structural and electrical properties of CNTs are advantageous for a range of industrial applications,[2] leading to CNTs becoming one of the major products of the nanoscale technologies in production volume terms. Their high-aspect ratio makes CNTs a useful industrial material and is also the basis for their similarity to asbestos, raising concern that the special pathogenic properties of asbestos may be mimicked.[1,3–5]

Exposure arising from the mining, milling, and industrial use of asbestos in the 20th century led to a global epidemic of cancer (eg, lung cancer and mesothelioma) and noncancerous diseases (eg, asbestosis, pleural effusions, and pleural plaques).[6] A large body of toxicological research produced a fiber pathogenicity paradigm that describes the characteristics of asbestos and other fibers that render them hazardous or nonhazardous. To be hazardous, a fiber must be thinner than 3 μm, longer than 10 to 20 μm, and biopersistent in the lungs and pleura, not dissolving or breaking into shorter fibers.[7] Sufficient exposure needs to be experienced for the number of long, thin, biopersistent fibers to reach a threshold dose at the target tissue for disease to be initiated. When these criteria are met and the threshold dose is exceeded, there can be a cascade of pathobiological processes, including recruitment of inflammatory cells, genotoxicity, mutation, and fibrosis in the target tissue,[6,8–10] leading to the spectrum of disease previously described.

Mesothelioma is almost exclusively found after asbestos exposure and is a particle response unique to fibrous particles.[8] Therefore, the potential effect that a new fiber-shaped particle like CNT may have on the mesothelium is a major concern in particle toxicology and occupational medicine. Previously, CNTs showed length-dependent inflammogenicity to the peritoneal mesothelium, similar to asbestos. After direct i.p. injection of long CNTs, an inflammatory response with granuloma formation and fibrosis occurred, whereas there was a negligible response to short and tangled CNTs.[11] As suggested in studies by Kane et al,[12] we concluded that long fibers are retained in the peritoneal cavity as a consequence of their inability to exit through stomata in the diaphragm, through which short fibers can egress. Herein, we developed a method to deliver CNTs into the more relevant pleural space to expose both the pleural mesothelial layers and assessed the inflammatory responses and the likely mechanism by which length-dependent pathogenicity might occur at this key site. The injection of long asbestos into the pleural space causes mesothelioma in rodents during a protracted period,[13] thus validating the intrapleural instillation model for studying premesothelioma processes.

Key to the acceptance of this model of direct exposure of the pleural mesothelium is the recognition that a proportion of all particles that deposit in the peripheral lung transit through to the pleura and normally exit through the stomata in the parietal pleura to the underlying lymphatic system and thereby to the mediastinal lymph nodes (LNs).[14] The recognition of this process is based on the presence of black spots (anthracotic areas) around stomata on the parietal pleura of almost all urban dwellers at autopsy,[15] with similar more severe lesions seen in miners,[16] reflecting their higher dust exposure. We hypothesized that particles and short CNTs that reach the pleural space would be readily cleared from the pleural space in the lymphatic flow through the stomata to the mediastinal LNs but that long fibers cannot negotiate the stomata and are, therefore, retained at the parietal pleura, initiating inflammation and pleural pathological conditions, including mesothelioma.[17] Therefore, the instillation of low doses of respirable dusts and fibers into the pleural space represents a credible approach to understanding the behavior of such particles in the pleura, where they are deposited in the lungs by inhalation.

Materials and Methods

Particle Panel

The panel of particles investigated consisted of five different samples of MWCNTs and three control particles that consisted of mixed-length amosite asbestos enriched for long fibers (50.36% fibers >15 μm and 35.25% fibers >20 μm), hereafter referred to as long-fiber asbestos (LFA); shortened amosite asbestos (SFA; 4.46% fibers >15 μm and 0.99% fibers >20 μm); and nanoparticle carbon black. The MWCNT panel comprised four commercially available CNTs and one sample produced in an academic research laboratory (University of Manchester, Manchester, UK) (Table 1). The MWCNT samples were categorized as long (NT_{long1} and NT_{long2}), short and tangled (NT_{tang1} and NT_{tang2}), or short and straight (NT_{short}), based on the manufacturer's description and physical characteristics observed using scanning electron microscopy (SEM), transmission electron microscopy, and light microscopy, as previously described by Poland et al.[11] The NT_{long1} sample (Mitsui & Co Ltd, Tokyo, Japan) was produced by catalytic chemical vapor synthesis using the floating reaction method. The NT_{long2} sample was produced in an academic research laboratory (University of Manchester, Manchester, UK) using a catalytic vapor discharge method with a ferrocene-toluene feedstock to grow nanotubes from iron catalysts held on a silica plate. These nanotubes grew aligned as mats, meaning they were straight and unentangled. The nanotubes were harvested from the mats using a razor blade, with some residual iron remaining within the nanotubes. We also included one commercially available NT_{short} and two curled and tangled nanotubes of different lengths (NT_{tang1}, which was cut to form predominantly short NT fibers; and NT_{tang2}, the original-length NT sample; NanoLab, Inc., Waltham, MA). These nanotubes were produced by catalytic vapor discharge with an iron and ceramic oxide (aluminosilicate) catalyst support that was removed using HCl and hydrofluoric acid treatment. Trace metals and endotoxin levels previously tested and reported by Poland et al were low and, thus, not considered to play a role in these studies. Quartz particles (DQ12), coal mine dust particles, and two samples of commercially available polystyrene beads (10- and 3-μm beads; Polysciences, Warrington, PA) were also used in this study. The mean particle diameters of DQ12 quartz and coal mine dust were measured by dynamic light scattering using a 90 plus Particle Size Analyzer (Brookhaven Instruments Corp., Holtsville, NY). Nickel nanowires (NiNWs) were fabricated by electrochemical template synthesis using alumina membranes (Anodisc 25; Whatman, Maidstone, UK), with an average pore diameter of 200 nm.[18,19] Short and long NiNWs with average lengths of 4.3 ± 1.0 μm and 24.0 ± 7.0 μm (values are ± SEM) respectively, were then examined by SEM (Carl Zeiss Ultra Plus, Hertfordshire, UK).

Transmission Electron Microscopy

A drop of SFA, LFA, or CNT sample (0.5 mg/mL in water) was placed on a grid with a support film of Formvar-carbon, excess material was blotted off with filter paper, and the material was examined under an FEI CM120 BioTwin Transmission Electron Microscope (Philips, Eindhoven, the Netherlands) using a Lab6 emitter. Images were captured using an AMT Digital Camera (AMT, Woburn, MA).

Light Microscopy

The particle panel was suspended in 0.5% bovine serum albumin (BSA; Sigma-Aldrich, Poole, UK) and saline at a concentration of 50 μg/mL and dispersed by sonication at 230 V, 50 Hz, and 350 W for 2 hours in an ultrasonic bath (FB11002; Fisherbrand, Thermo Fisher Scientific, Inc., Waltham, MA). The particle suspensions, 10 μL, were placed on glass slides. Glycerol, 10 μL (Sigma-Aldrich), was added to each slide and mixed with the particle suspension to reduce the flow of particles and enable a clear picture to be captured. A glass coverslip was placed over the suspensions and sealed. Images were captured at ×40 magnification using QCapture Pro software (Media Cybernetics Inc., Bethesda, MD).

Intrapleural Injection and Lavage

Samples were prepared for *in vivo* use by ultrasonication in a sterile 0.5% BSA-saline solution and were injected into the pleural cavity of female C57Bl/6 mice (aged 8 weeks) at a dose of 50 μg/mL (100 μL; total dose, 5 μg per mouse). Injection directly into the pleural space without perforating the lung was enabled by the addition of a sleeve over the tip of the 27-Gauge, which prevented the needle from passing through the pleural space into the lung. After 24 hours ($n = 5$), 7 days ($n = 4$), 4 weeks ($n = 4$), 12 weeks ($n = 4$), and 24 weeks ($n = 5$), the mice were euthanized by asphyxiation in 100% CO_2 and the pleural space was lavaged using three 1-mL washes of sterile saline kept on ice. The lavage fluid was centrifuged at 123 × *g* for 5 minutes at 4°C in a Mistral 3000i centrifuge (Thermo Fisher Scientific, Inc.) to separate the cellular fraction, and the supernatant protein content was established using the bicinchoninic acid protein assay (Sigma-Aldrich). The cell pellet was resuspended in PBS, and a total cell count was then performed using a NucleoCounter (ChemoMetec, A/S, Allerød, Denmark). Differential cell counts were performed on cytocentrifugation preparations and stained with a Diff-Quik stain set (Dade Behring Gmbh, Marburg, Germany).

Tissue Dissection

The lower right posterior portion of the chest wall was carefully removed from the mice after lavage of the pleural space. This region of the parietal pleura was identified by Shinohara[20] as a region rich in stomata. The tissue was washed in ice-cold saline and placed overnight in methacarn fixative (60% methanol, 30% chloroform, and

10% glacial acetic acid). Samples were embedded in paraffin, sectioned, and stained with H&E for gross pathology, picrosirius red to stain collagen, and Ki-67 proliferation marker (rabbit polyclonal anti–Ki-67, ab15580; Abcam, Cambridge, UK) ($n = 3$ per treatment). The same region of the chest wall removed from one mouse per treatment for surface analysis by SEM was fixed in 3% glutaraldehyde–0.1 mol/L sodium cacodylate (pH 7.2) buffer. After overnight incubation in fixative, the area of interest was excised from the surrounding tissue. The specific region of chest wall that was examined corresponded to an area 1 × 0.5 cm along the spine, which encompassed the lower six ribs and intercostal spaces.

Quantification of Lesions

The excised tissue was dehydrated through graded alcohol (ethanol) and embedded on edge in paraffin. Sections of the chest wall, 4 μm, were stained with H&E; and serial images were taken at ×10 magnification using QCapture Pro software (Media Cybernetics Inc., Bethesda, MD). The images were seamlessly realigned using Photoshop CS3 (Adobe Systems Inc., San Jose, CA) to provide a high-resolution image of the large sections of chest wall. By using calibrated Image-Pro Plus software (Media Cybernetics Inc.), the total length of each chest wall section along the mesothelium was measured to adjust for any differences in size between reconstructed sections. By using the same software, the area occupied by lesions was measured and expressed as lesion area per unit chest wall length ($\mu m^2/\mu m$). The collagen content was measured using Image-Pro Plus software by quantifying the red pixels in each section and expressed as area of positive collagen staining per unit length of chest wall (mm^2/mm) ($n = 3$).

Scanning Electron Microscopy

The excised diaphragm was stained with osmium tetroxide before critical point drying, mounted, and gold sputter coated before examination by SEM using a Hitachi S-2600N digital SEM (Oxford Instruments, Oxfordshire, UK).

Whole-Body Imaging of NT_{short}–DTPA [^{111}In]-Injected Animals by Single-Photon Emission Computed Tomography

NT_{short}-NH_3^+ samples were obtained following the procedure by Li et al[21] and incubated with diethylenetriaminepentaacetic acid (DTPA) for 48 hours at 50°C. The NT_{short}-DTPA was recovered by centrifugation and labeled with the radioactive tracer [^{111}In]Cl_3 (Amersham Pharmacia Biosciences, Buckinghamshire, UK). The [^{111}In]Cl_3 alone, used as a control, was also subjected to the same conditions of the labeling reaction. Balb/C mice were anesthetized by isoflurane inhalation. Each animal received an intrapleural injection of 100 μL containing 5 μg of NT_{short}-DTPA[^{111}In], with an activity of approximately 3 to 5 MBq. [^{111}In]DTPA with the same activity was injected for comparison. Within 1 hour of injection (t = 0 to 1 hour) and at t = 23 to 24 hours, mice were imaged using the Nano-SPECT/CT scanner (Bioscan, Washington, DC). Single-photon emission computed tomographic (SPECT) images were obtained in 16 projections over 40 to 60 minutes using a four-head scanner with 1.4-mm pinhole collimators. CT scans were taken at the end of each SPECT acquisition, and all images were reconstructed with MEDISO software (Medical Imaging Systems, London, UK). Fusion of SPECT and CT images was performed using PMOD software (PMOD, Zurich, Switzerland).

Quantification of LN NiNW Burden

NiNW samples were prepared and injected into the pleural cavity following the same protocol as was used for CNT samples. Mice ($n = 3$) were sacrificed 24 hours after injection, and the mediastinal LNs were carefully excised, fixed, sectioned, and stained with picrosirius red to allow for clear visualization of the NiNW. Six sequential sections were taken from each LN, giving 18 sections per treatment group. Images were taken at ×10 magnification for tissue area measurement and ×40 magnification for fiber counting using QCapture Pro software (Media Cybernetics Inc.).

Statistical Analysis

All data are shown as the mean ± SEM and were analyzed using one-way analysis of variance. Multiple comparisons were analyzed using the Tukey–honestly significant difference method, with values of $P < 0.05$ considered statistically significant (Instat; Graphpad Software Inc., San Diego, CA).

Results

CNT-Fiber Panel

To specifically assess the role of length in the pleural response to CNTs, we assembled a panel[11] that consisted of long, short, and short and tangled CNTs; control LFA and SFA; and nanoparticle carbon black as a particulate carbon control. The morphological features of the CNT samples were determined by transmission electron microscopy analysis (Figure 1). Light microscopy analysis of the CNT panel and control samples, dispersed by ultrasonication in 0.5% BSA-saline, before administration, showed the presence of fibers in the LFA, NT_{long1}, and NT_{long2} samples; the SFA, NT_{short}, NT_{tang1}, and NT_{tang2} samples were composed of small aggregates of respirable size (Figure 1). Members of the CNT panel were administered by injection directly into the pleural space through the chest wall in unanesthetized mice, using a modified fine-bore needle to prevent injection into the lung; both short- and longer-term responses were examined.

Acute Inflammatory Response to Intrapleural Injection of the CNT-Fiber Panel

The acute inflammatory response produced by instillation of the CNT-fiber panel directly into the pleural space was

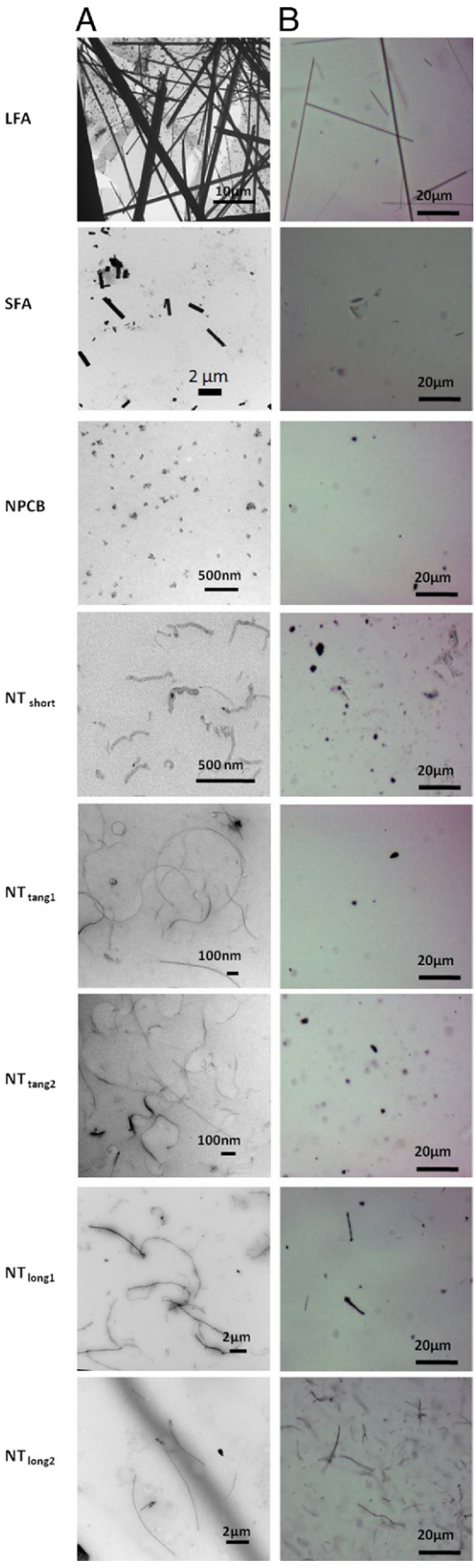

measured at 24 hours by lavaging the pleural space and counting the cell types. Only intrapleural injection of the samples containing long fibers (ie, LFA, NT_{long1}, and NT_{long2}) caused a significant increase in total cell number (Figure 2A) in the lavage fluid. We also determined the number of granulocytes, which included mainly neutrophils and a few eosinophils, as an indicator of acute inflammation in the lavage fluid. Only mice that were injected with long CNTs or asbestos showed significantly increased granulocytes in the pleural lavage compared with the vehicle control (Figure 2B). Mice injected intrapleurally with SFA, nanoparticle carbon black, NT_{short}, NT_{tang1}, or NT_{tang2}, which did not contain long fibers, failed to show any significant increase in the numbers of pleural granulocytes compared with controls (Figure 2B). Protein levels in the lavage fluid, which are indicative of the fluid exudate of inflammation, reflected the pattern seen with granulocyte influx (Figure 2C). The acute inflammatory response in the pleural space was examined up to 7 days after intrapleural injection, for representative long (NT_{long2}) and short (NT_{tang1}) CNT samples (Figure 2D). The increase in the number of granulocytes seen in the pleural lavage of mice injected with NT_{long2} was maintained up to 7 days, with no reduction in the extent of the inflammation, whereas the few granulocytes in NT_{tang1}-treated mice had waned to control levels by 7 days (Figure 2D). By 4 weeks, the number of granulocytes in the NT_{long2}-treated mice was greatly reduced but remained higher than the level of granulocytes in the vehicle control or NT_{tang1}-treated mice up to 24 weeks after injection.

Parietal Pleura Histological Features up to 7 Days

A histological examination was performed on parietal pleura samples from mice injected with short and long CNT exemplars (NT_{tang1} and NT_{long2}, respectively) at 1 and 7 days after intrapleural instillation to examine the development of the early inflammatory mesothelial response (Figure 2E). Aggregates of inflammatory cells were present on the pleural surface in both NT_{tang1} and NT_{long2} samples at 1 day, but by 7 days, the parietal pleura from mice instilled with NT_{tang1} looked completely normal. There was evidence of increasing inflammatory cell accumulation and long CNT retention only in NT_{long2} samples at 7 days (Figure 2E).

Parietal Pleura Histological Features up to 24 Weeks

To investigate the development of the inflammatory lesions on the parietal pleura over time, the parietal

Figure 1. CNT panel. **A:** Transmission electron microscopy (different magnifications used). **B:** Light micrographs of each member of the CNT panel. For light micrographs, CNTs and fibers were dispersed by ultrasonication in 0.5% BSA-saline at a concentration of 50 µg/mL to the standard degree of dispersion used for intrapleural injection. NPCB indicates nanoparticle carbon black.

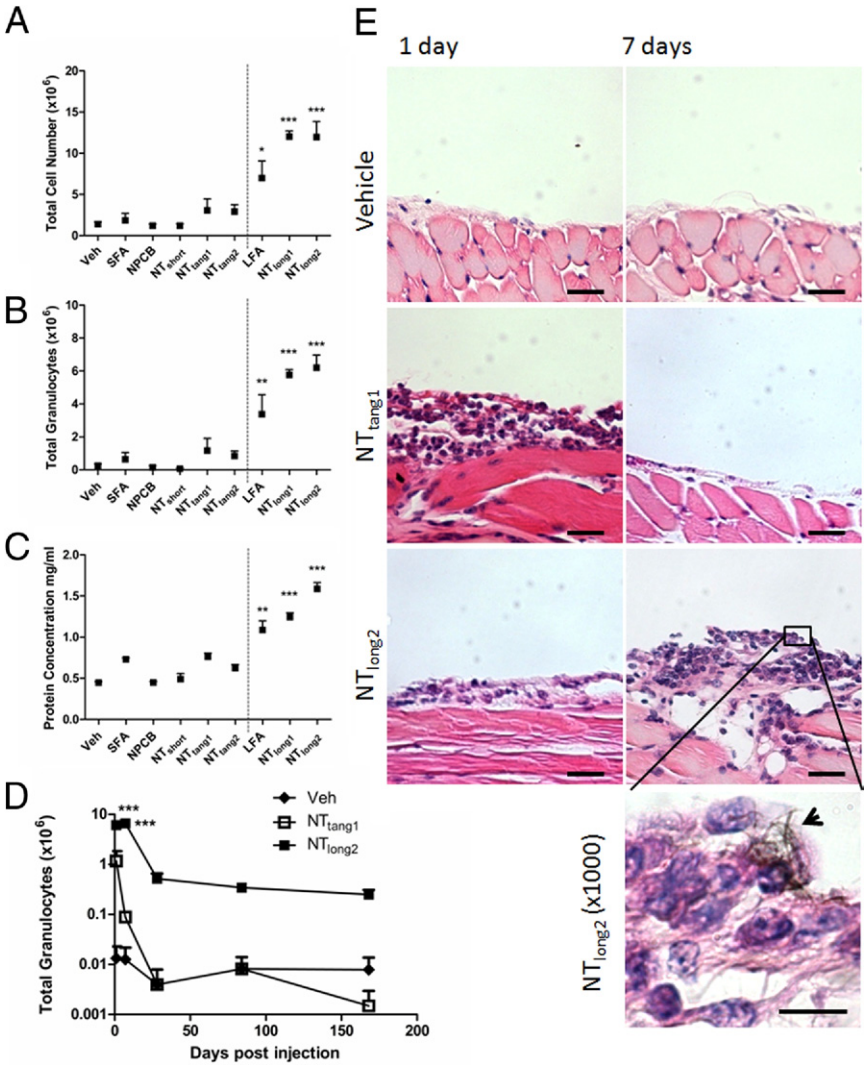

Figure 2. Acute inflammatory response to intrapleural injection of CNT. Total cell number (**A**), total granulocytes (**B**), and total protein (**C**) were measured in the lavage fluid of mice injected with 5 μg of CNT and controls at 24 hours after injection. Total granulocytes (**D**) were measured in lavage fluid of mice treated with either NT_{tang1} or NT_{long2} up to 168 days (24 weeks) after injection. $^{*}P < 0.05$; $^{**}P < 0.01$; $^{***}P < 0.001$ versus vehicle (Veh) control. Data represent mean ± SEM ($n = 5$ mice per treatment group). **E:** Histological examination of chest wall samples from mice injected with NT_{tang1} and NT_{long2} at 1 and 7 days after injection. Aggregates of inflammatory cells are present in both NT_{tang1} and NT_{long2} samples at 1 day but only in NT_{long2} samples at 7 days. The **arrowhead** indicates long CNT aggregates in ×100 magnification of NT_{long2} (7-day sample). Scale bar = 20 μm. NPCB indicates nanoparticle carbon black.

pleura was further examined at 4, 12, and 24 weeks after injection of NT_{tang1} and NT_{long2}. At all these points, mice treated with vehicle control and with the NT_{tang1} sample had a single layer of mesothelial cells along the parietal pleural surface with no inflammatory involvement. In contrast, parietal pleura sections from mice treated with NT_{long2} showed the presence of a fibrotic layer over the parietal pleura, which continued to increase in thickness over time from 4 to 24 weeks after injection (Figure 3A). The lesions had high collagen content, determined by staining with picrosirius red; and displayed stratified reticular morphological features separated by cellular aggregates. The area of lesion development and the collagen content of the lesions were quantified (Figure 3B). High-power views of the lesion at 24 weeks after injection show vascularization of the lesions, with lymphocyte infiltrates surrounding the blood vessels (Figure 3C). The upper surface of the lesion also appeared to be covered by plump, reactive, and proliferating mesothelial cells. Aggregates of long CNTs were seen in the deeper layers of the developing lesions, reflecting the site of CNT retention in the parietal pleura (Figure 3A). No CNT aggregates were seen in the parietal pleural sections of NT_{tang1}-treated mice. Similar lesion development was seen on examination of the pleural face of the diaphragm of the NT_{long2}- but not the NT_{tang1}- or vehicle control–treated mice (data not shown).

SEM Analysis of the Parietal Pleural Surface

The surface appearance of the parietal pleura was examined by SEM in areas known to have high stomatal density at 1, 4, 12, and 24 weeks in mice exposed to long and short CNTs. The vehicle control samples displayed a continuous normal mesothelium at every point (Figure 4, A–D), with no leukocyte aggregates. NT_{tang1}-treated mice showed a mild response at 1 week, characterized by small areas of leukocyte aggregation on the mesothelial surface (Figure 4E), a response that had resolved by 4 weeks; only a normal mesothelium was seen at subsequent points (Figure 4, F–H). In contrast, in NT_{long2}-treated mice, more extensive and persistent lesions developed (Figure 4, I–L). At 1 week, we observed a large mat of leukocytes forming an almost contiguous layer across the pleural

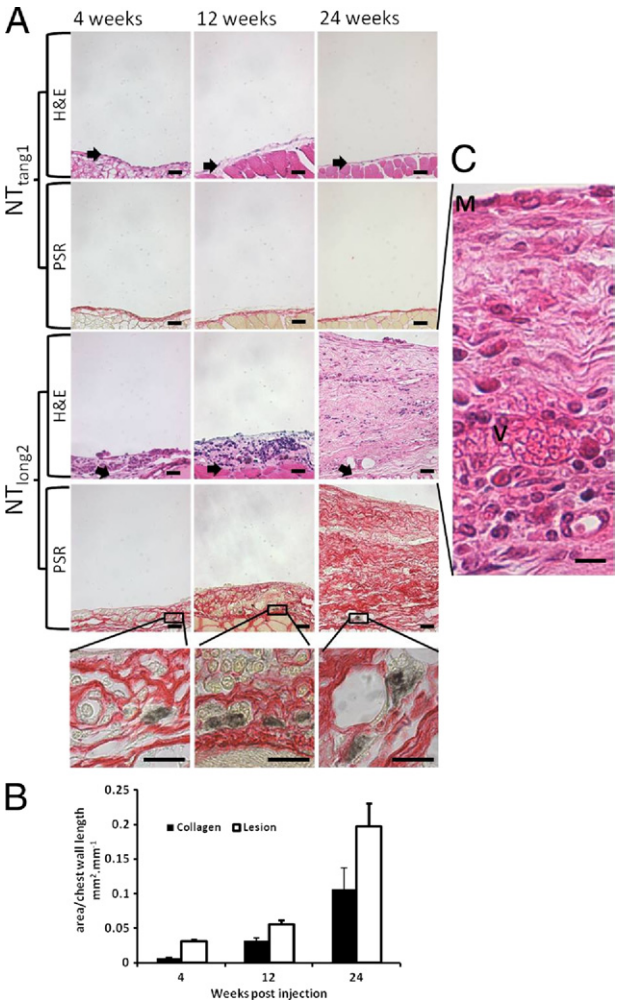

Figure 3. Fibrotic lesion development. **A:** Parietal pleura of the chest wall of mice treated with NT_{tang1} and NT_{long2} were examined histologically at 4, 12, and 24 weeks after injection. Sections were stained with both H&E for gross morphological features and picrosirius red for collagen. **Arrows** indicate level of original mesothelium. Call outs to a high-power view show aggregates of CNT present within the fibrous lesion at each point. Scale bar = 20 μm. **B:** Lesion size and collagen content were quantified for the NT_{long2} samples and expressed as area per length of chest wall section (mm^2/mm). Data are represented as the mean ± SEM (n = 3). **C:** High-power views of the lesion at 24 weeks show the lesion is vascularized (V) and covered with a layer of mesothelial cells (M). Scale bar = 20 μm.

surface, bound with fibrin (Figure 4M). By 4 weeks, the lesion had decreased in size and had developed well-defined boundaries, with apparently normal mesothelium in between. Fibrin was still present and appeared to be involved in the adherence of the aggregates to the mesothelium. By 12 weeks, the lesions were more contained within the intercostal depressions. High-power views (Figure 4, M–P) showed no fibrin in association with the leukocytes by 12 and 24 weeks and the apparent attempt by mesothelial cells to regrow over the surface of the lesions. At 24 weeks, papillae or tongue-like structures composed of cell aggregates, which extend from the surface of the mesothelium, can be seen. A high-power view shows these papillae to contain and be covered by mesothelial cells, as identified by the presence of microvilli on the cell surface.

Cellular Proliferation in the Mesothelium of the Parietal Pleura

The progressive covering of lesions by mesothelial cells, as observed from the SEM analysis, implies proliferation of cells along the parietal pleural surface. Sections of parietal pleura and diaphragm from vehicle control–, NT_{tang1}-, and NT_{long2}-treated mice 24 weeks after injection were stained with Ki-67 antibody (Figure 5). Positive Ki-67 staining, which identifies actively proliferating cells, was only observed along the mesothelial surface of the pleural mesothelium of NT_{long2}-treated mice and not in mice treated with short nanotubes (NT_{tang1}). The positive-staining cells were mostly concentrated along the mesothelial layer of the parietal pleura and on the pleural face of the diaphragm in association with the layer of fibrosis.

Size-Related Pleural Retention of Compact Particles

We hypothesized that the inflammatory effects of long CNTs and long fibers in general arise as a consequence of retention at stomata whose maximum diameter is 10 μm (Figure 6A). To test this hypothesis, we used two well-known proinflammatory particles that are small enough to exit through the stomata (ie, quartz and coal mine dust) and polystyrene beads in two sizes (3 and 10 μm, Figure 6B). All of these particles, except the 10-μm beads, were small enough to exit the stomata. We hypothesized that only the 10-μm beads should be retained and would, therefore, elicit inflammation in the pleural space. When instilled into the pleural space at the same mass dose as the CNTs, no response was seen with the quartz or coal mine dust, despite their reactivity within the lung, or the 3-μm beads. In contrast, the 10-μm beads that are too big to exit through the stomata elicited inflammation at 24 hours (Figure 6C).

Length-Dependent Retention of Fibers

We used two indirect approaches to assess the hypothesis that, similar to the large polystyrene beads, long CNTs were retained in the pleural space while short fibers were cleared through the stomata.

SPECT/CT Imaging of Radiolabeled Short CNT Fibers

Dynamic SPECT/CT imaging was used to visualize the fate of radiolabeled short CNTs (NT_{short}-DTPA[^{111}In]) after direct injection into the pleural space. Imaging during the first hour after administration of the radiolabeled CNTs indicated widespread diffusion of the signal, largely confined to, and throughout, the pleural cavity (Figure 7A). Even within 1 hour and increasingly thereafter, the short CNTs accumulated in the cranial mediastinal LNs (two bilateral LNs located lateral to the thymus). At 24 hours after administration, the signal from NT_{short} was localized almost exclusively within these LNs (Figure 7B). The control [^{111}In]DTPA label alone showed rapid

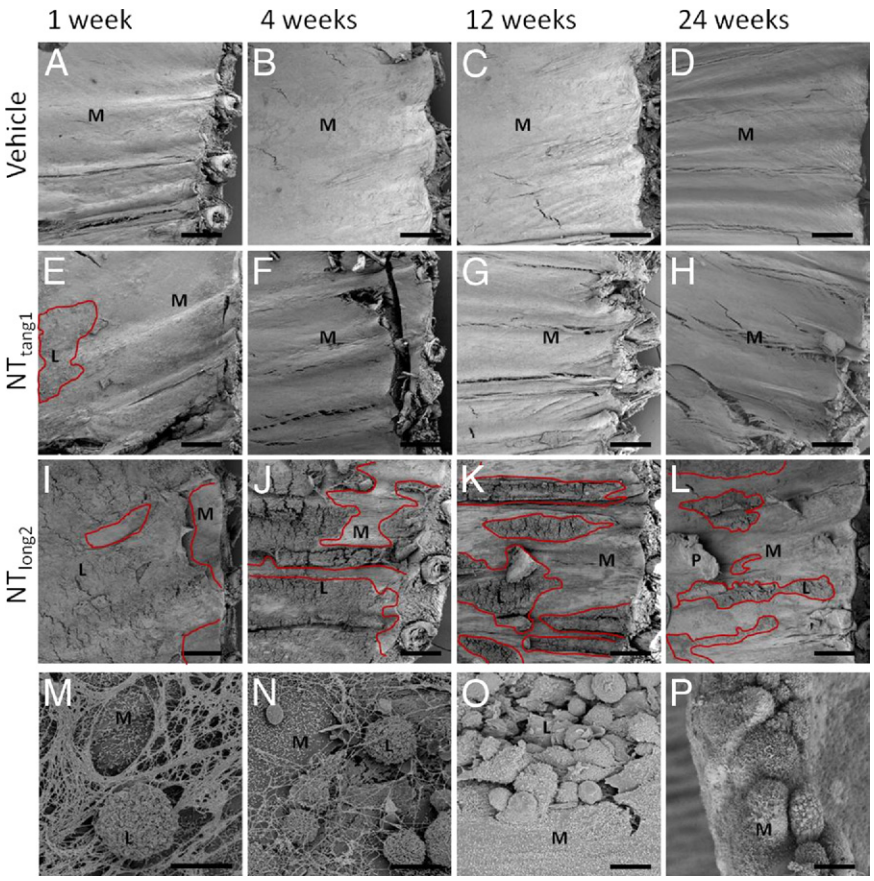

Figure 4. SEM analysis of lesion development over time. The surface of the chest wall parietal pleura was examined by SEM at 1, 4, 12, and 24 weeks after injection. **A–L:** Low-magnification images (×30) show continuous normal mesothelium (M) in vehicle control–treated mice. L indicates the inflammatory lesions (also outlined in red), which are mild and resolve quickly in NT_{tang1}-treated mice or are extensive and persistent in NT_{long2}-treated mice. P indicates papillae, tonguelike extensions from the mesothelium, in NT_{long2}-treated samples. Scale bar = 500 μm. **M–P:** High-power view of the lesions present in NT_{long2}-treated mice shows the changing nature of the lesion over time from fibrinous leukocyte aggregates at early points to the progressive resurfacing of the lesion by mesothelial cells. The papillae present at 24 weeks appear to contain and be covered by mesothelial cells, as identified by the presence of microvilli. Scale bar = 10 μm.

translocation to the bladder, with almost the entire dose cleared within the first hour after intrapleural administration (Figure 7C). This demonstrated the stability of *in vivo* radiolabeling of short nanotubes and their clearance from the pleural cavity to the specific mediastinal LNs.

Visualization of Clearance of Long and Short Fibers in Cranial Mediastinal LNs

We took advantage of the knowledge gained from the SPECT/CT that the destination of fibers cleared through stomata is the cranial mediastinal LNs and examined the fiber burden in these LNs 24 hours after intrapleural injection of short and long CNTs (Figure 7E). The results showed apparently greater CNTs in the LNs in NT_{short}-treated mice than in NT_{long2}-treated mice. However, these results were qualitative because of the difficulties of counting the small CNTs in lymphoid tissue; interpretation was further confounded by the presence of short fibers in the NT_{long2} samples (approximately 15% of the fibers were <15 μm).

To gain further evidence, we examined clearance to the mediastinal LNs using short and long versions of alternative high-aspect ratio nanowires made of nickel. NiNWs are more readily visualized histologically than CNTs and have the additional benefit that they are synthesized in tight-size categories, with few short fibers in the long sample and no long fibers in the short sample (Figure 8A). This narrow size distribution range is mainly because of the controlled fabrication process used. The injection of these NiNW samples into the pleural space resulted in a similar length-dependent acute inflammatory response (Figure 8B). After injection into the pleural space, we hypothesized that, as was the case with CNTs, exclusively short NiNWs would appear in the LNs on clearance from the pleural space while the predominately long NiNWs would be retained in the pleural space and, therefore, would not accumulate in the draining LNs. Quantification of the number of NiNWs in histological sections of excised mediastinal lymph tissue showed that significantly more fibers have migrated from the pleural space to the LNs in mice treated with short compared with long NiNWs (Figure 8, C and D). This completely supports the hypothesis that long fibers reaching the pleural space are selectively retained, never reaching the mediastinal LNs, whereas short fibers are small enough to be cleared through the parietal stomata to the mediastinal nodes.

Discussion

To our knowledge, for the first time, we report a clear length-dependent inflammogenicity for CNTs when injected directly into the pleural space of mice. At the initial time of 24 hours, LFA and SFA were included as positive and negative controls, respectively; for the end points examined, the responses to the CNTs followed this length-dependent pattern. Exposure to long CNTs first

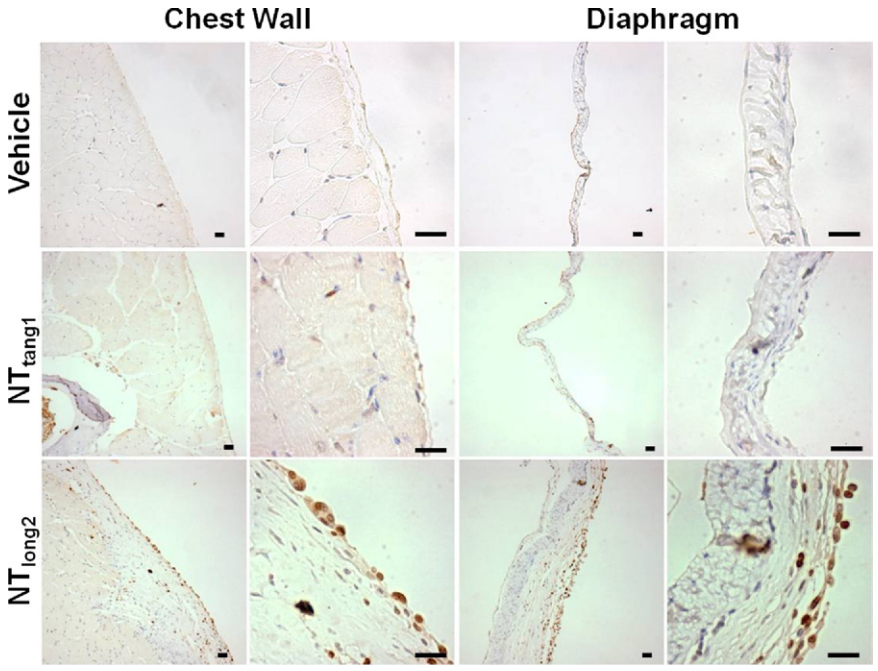

Figure 5. Cellular proliferation along the mesothelium of CNT-treated mice. Cellular proliferation along the parietal pleural of the chest wall and diaphragm was examined in mice treated with vehicle control, NT_{tang1}, and NT_{long2} at 24 weeks after injection. Sections were stained with anti–Ki-67 antibody, a marker for actively proliferating cells. Ki-67–positive staining was only detected along the mesothelium in mice treated with NT_{long2}. Scale bar = 20 μm.

caused an acute inflammatory response, characterized by granulocyte influx, mostly neutrophils, and increased protein concentration in the pleural fluid, followed by the progressive development of fibrotic lesions along the parietal pleura and proliferation in the mesothelial layers. Short CNTs did not elicit a significant inflammatory reaction at any point examined and, indeed, the results obtained from short CNT-treated mice mirrored those of the vehicle controls. These results suggest that, like asbestos, the toxicity of CNTs for the pleura adheres to the fiber pathogenicity paradigm[11] regarding the role of length in this model of direct pleural exposure.

Because of the importance of respirability in delivering particles to the lung periphery, where they can be translocated to the pleural space, it is vital to use well-dispersed particles in our studies that presuppose that the particles reach the lung periphery and the pleura. By using BSA and ultrasonication, we were able to produce well-dispersed respirable-sized suspensions of all of the particles, with fiber-shaped particles being visible by light microscopy in the LFA, NT_{long1}, and NT_{long2} samples. Given the resolution of the light microscope, we assume that the visible fibers in the CNT preparation are ropes of intertwined MWCNTs.[11] After injection into the pleural space, we detected an inflammatory response to the long, but not short, CNTs. Also, in a time course with one of the long CNT samples, we found the inflammation elicited was sustained over 1 week at the level seen at 1 day. Given the basic premise of toxicology that response follows dose, we presumed that the long CNTs were retained in the pleural space, where they are a stimulus to inflammation, whereas the short CNTs are cleared.

Length-dependent pathogenicity of asbestos and other fibers is one of the defining properties of the fiber pathogenicity paradigm[17] and has been documented in several models *in vivo*[9,22–25] and *in vitro*,[25–27] whereas frustrated or incomplete phagocytosis by macrophages has been implicated as a mechanism leading to inflammation with long fibers[26] and CNTs.[28] Length-related retention was first advanced by Kane et al[12] to explain length-dependent asbestos inflammation in the peritoneal cavity. In fact, the peritoneal and pleural cavities have similar mechanisms of clearance, involving fluid flow out of the respective cavities through stomata that are highly size selective.[17]

Clearance from the pleural space is via passive removal of the particles in the flow of pleural fluid out through stomata in the parietal pleura, into the lymphatic system.[14] Stomata (diameter, 3 to 10 μm) act as a "sieve" for drainage from the pleural space and are found along the parietal pleura of the chest wall and diaphragm, in highest abundance in the most caudal posterior intercostal spaces in rodents.[20] Failure to clear the long CNTs from the pleural space, as suggested by the presence of CNT aggregates in the lesions of long CNT-treated mice, forms the basis of a proposed mechanism of long-fiber pathogenicity in the pleural space (ie, retention of long fibers at these points of egress of the lymph), resulting in an inflammatory response. Mesothelioma arises on the parietal pleura,[29] the site of retention of the long-fiber dose. We found that the inflammation produced by long CNTs was sustained and was similar on day 7 to that seen on day 1. This is in contrast to the tempo of inflammation seen in the peritoneal space to the same long CNT sample, where the inflammation waned considerably over 1 week after long CNT and long asbestos.[11] The persistence of inflammation in the pleural space may be a consequence of the conditions there, where movements of the chest wall and close apposition of the parietal and visceral pleurae enhance the interactions between long CNTs and the mesothelium at their points of retention. Sustained inflammation arising from retained

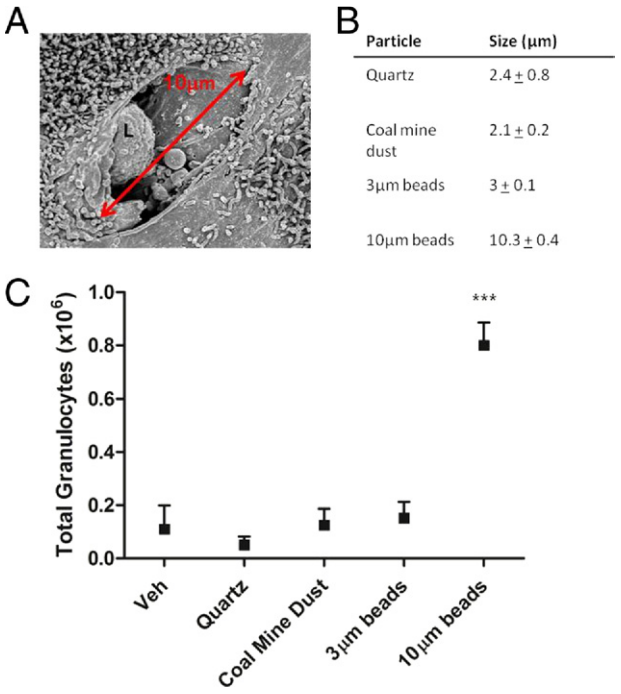

Figure 6. Size-dependent inflammatory response to compact particles in the pleural space. **A:** SEM image of a lymphatic stoma (diameter, 10 μm) found on the parietal pleura of the internal chest wall of a mouse. L indicates a leukocyte passing through the stoma. **B:** Mean size of particles as measured by dynamic light scattering. Data are represented as mean ± SEM. **C:** Total granulocytes measured in pleural lavage fluid of mice 24 hours after injection of "inflammatory" particles: quartz (DQ12) and coal mine dust or 3- and 10-μm beads. Only the 10-μm beads caused a significant increase in granulocytes. Data are represented by mean ± SEM. $^{***}P < 0.001$ versus vehicle (Veh) control.

long fibers produces an inflammatory response at the sites of retention. These foci of inflammation were most evident in the SEM images of the parietal pleura that showed leukocyte aggregates over a relatively large area of the face of the parietal pleura in regions documented to have large concentrations of stomata. The relatively high doses used in our studies produced these anticipated large areas of leukocyte accumulation, which lessened somewhat with time, but only remained substantial in the case of the long CNTs. Analogous lesions have been reported on the mesothelium of the peritoneal cavity after instillation of long asbestos fibers[30] and, similar to what we observed herein, showed a tendency for the lesions to be covered by mesothelial cells with time after instillation.[30] Multiple instillations of asbestos into the rat pleural space, known to cause mesothelioma, were used in one study[31] to examine the changes at the pleural mesothelium observed by SEM over 24 months, leading up to mesothelioma development. Leukocytic lesions and foci of mesothelial proliferation, similar to those seen with the long CNTs, were also documented on the face of the parietal pleura. Hyperplastic areas of mesothelium, reported by Vasilieva et al,[31] were evident in our study, highlighted by the Ki-67 antibody staining, which showed dramatic increases in proliferation in the mesothelial and submesothelial tissues only in mice exposed to long CNTs. Recently, inhalation of amphibole asbestos produced similar leukocytic lesions on the pleural face of the diaphragm, detected by electron microscopy.[32] This latter study is particularly important because it supports our contention[17] that a proportion of fibers that deposit in the distal lung enter the pleural space but that only long fibers are retained, causing a reaction. There are additional structures present along the pleural mesothelium referred to as *milky spots*, which contain accumulations of lymphocytes and macrophages that are reported to be important in the response to pleural injury. These milky spots are found in abundance along the mediastinum and in the vicinity of the pulmonary ligaments.[33] The examination of the parietal pleura reported herein focused on the caudal dorsal intercostal spaces, regions reported to be rich in stomata[14,20]; no milky spots were encountered in the tissue sections examined. However, considering their composition of macrophages and lymphocytes, it is likely that the cells resident in the milky spots contributed to the inflammatory responses reported herein. The accumulation of inflammatory leukocytes at the points of retention of long fibers at the stomata and

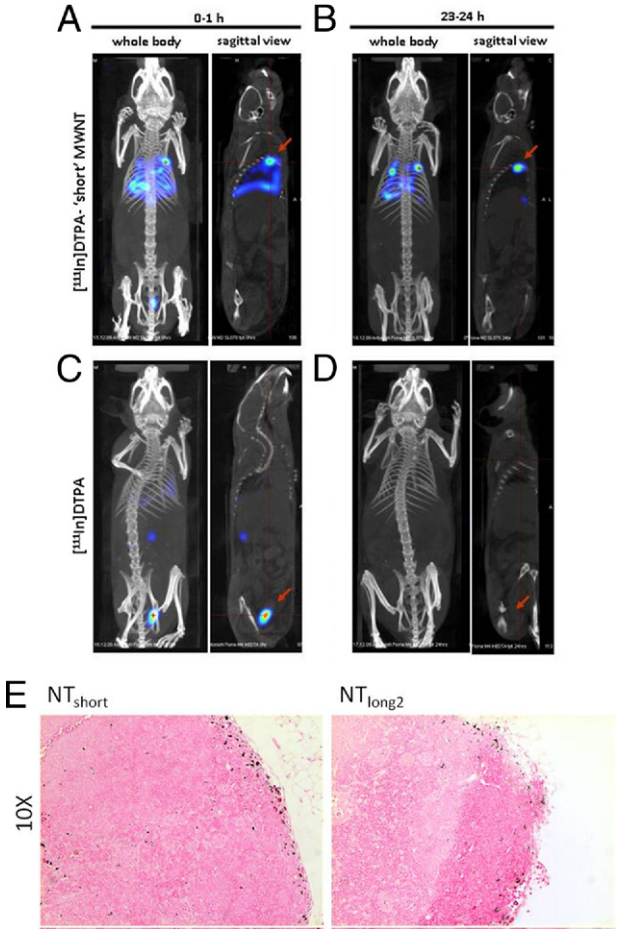

Figure 7. Clearance of CNTs from the pleural space. Whole-body Nano-SPECT/CT imaging of NT_{short}-DTPA[^{111}In]. Imaging was performed immediately (0 to 1 hour) and 1 day (23 to 24 hours) after intrapleural administration of 5 μg of NT_{short}-DTPA[^{111}In] (**A** and **B**) or [^{111}In]DTPA (**C** and **D**). The scanning duration was 60 minutes. SPECT/CT-fused images of the whole body (anterior view) and sagittal planes are shown. **Arrows** indicate the cranial mediastinal LNs (**A** and **B**) and bladder (**C** and **D**) in the case of NT_{short}-DTPA[^{111}In] and [^{111}In]DTPA, respectively. **E:** Cranial mediastinal LNs removed from mice intrapleurally injected with nonradiolabeled long and short CNTs sectioned and stained with H&E.

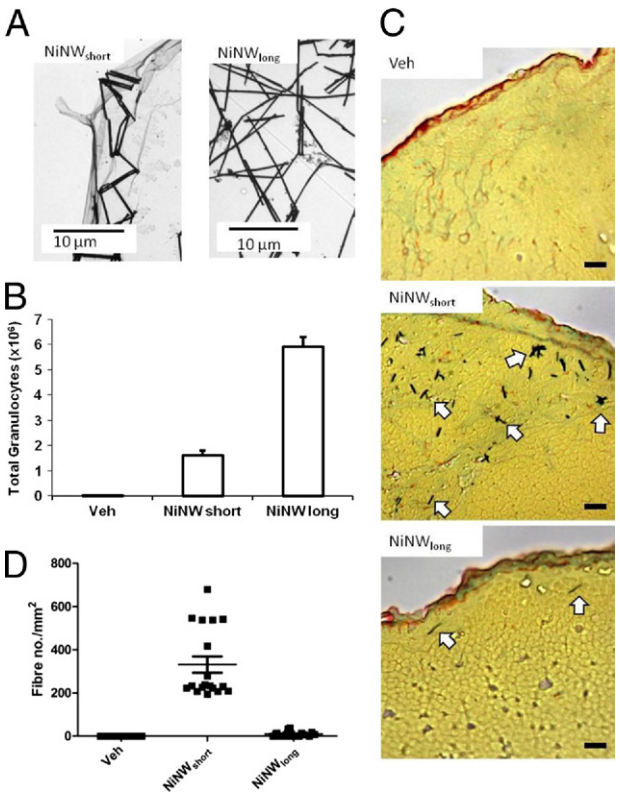

Figure 8. Clearance of short NiNWs to the cranial mediastinal LNs. **A:** Transmission electron microscopy images of short and long NiNWs. **B:** Total granulocytes in the pleural lavage fluid 24 hours after injection with vehicle (Veh) control or short or long NiNWs. $^{***}P < 0.001$ versus Veh control. **C:** Histological sections of cranial mediastinal LNs excised from mice 24 hours after intrapleural injection of short or long NiNWs ($n = 3$) and stained with picrosirius red to make the NiNWs more visible. **Arrows** indicate NiNWs. Scale bar = 10 μm. **D:** Fiber number per square millimeter of LN tissue was determined by counting the total number of fibers from six sequential sections of each cranial mediastinal LN and measuring the area of tissue in each section. Data are presented as the mean ± SEM ($n = 3$ mice per treatment group).

mesothelial proliferation at these foci are likely to result in an environment rich in cytokines, growth factors, and oxidants. This environment is fertile for producing further mesothelial injury, proliferation, remodeling, mutation, and, ultimately, transformation.

Some confirmation for this hypothesis was obtained in the form of a rapidly developing florid submesothelial fibrotic response that developed over the pleural surfaces only in animals treated with long fibers. This layer of fibrosis formed on the diaphragm and the parietal pleura, both regions rich in stomata, where long fibers would be expected to be retained. The fibrosis that formed was progressive, becoming approximately 20 times thicker and having more collagen between 1 and 24 weeks. These lesions were similar to those seen in the peritoneal cavity with long fibers[11,30] and have some similarities to pleural plaques[34] in the layered parallel reticular network of collagen that characterizes the lesions.

We investigated the validity of our model for retention-dependent inflammation by using compact particles and examining their clearance and inflammatory potential. Quartz and coal mine dust are small particles (<3 μm) that would reach the periphery of the lung and could enter the pleural space. They are known to be inflammogenic in the lungs after inhalation,[35,36] playing a causative role in the pathogenesis of silicosis and pneumoconiosis.[37] The lack of response to these highly inflammogenic particles in the pleural exposure model can be explained by their small size (ie, they are rapidly cleared from the pleural space in the flow of pleural fluid). Based on these studies, we undertook a simple proof-of-concept study to investigate the single parameter of particle size and its potential connection to inflammation in the pleural space using two monodispersed samples of polystyrene beads that were identical in composition but different in diameter. As expected at the same mass dose (meaning many more small beads), the larger 10-μm beads, which are approximately the maximum stomatal diameter, initiated an acute inflammatory response, whereas the smaller 3-μm beads did not initiate this response. Although a 10-μm bead is too large to ever reach the distal lung and pleural space on inhalation, the inflammatory response to the 10-μm beads injected directly into the pleural space demonstrates the role that size-restricted clearance from the pleural space plays in the initiation of an inflammatory response to particles or fibers.

Normally, the elutriating effects of the lung serve to allow only particles smaller than approximately 5 μm and, therefore, smaller than the diameter of the pleural stomata to reach the distal lung and translocate to the pleural space. Particles of this size will be easily cleared in the flow of pleural fluid, where they drain to the mediastinal, parasternal, and hilar LNs.[38] However, fiber respirability is a function of aerodynamic diameter, dictated mostly by actual diameter as air-borne fibers align themselves parallel to the airflow in the lungs. Therefore, it is the diameter (not the length) of fibers that affects transit through the lungs, allowing high-aspect ratio particles like CNTs, which may have a diameter in the nanometer range but a length extending to tens of micrometers, to deposit in the distal regions of the lung.[17] Indeed, the distal deposition of CNTs was shown by Ryman-Rasmussen et al,[39] who reported the presence of CNTs in the subpleural tissue of the lung after a single inhalation exposure in mice. Translocation of particles and fibers from the distal lung to the pleural space is not well understood. Mercer et al[40] showed MWCNTs penetrating the visceral pleura of the lung and extending into the pleural space over several points after a single pharyngeal aspiration exposure in mice, suggesting a direct route of translocation. An alternatively suggested mechanism of translocation is the primary translocation of fibers into the blood, from where they can potentially move to any area of the body, including the pleural space[41]; however, that mechanism was not investigated herein. The movement of distally deposited CNTs into the pleural space is in agreement with literature suggesting that a proportion of all particles deposited distally will pass into the pleural space, thus validating the use of a direct pleural exposure model that bypasses the lung to answer the more pertinent question of how the CNTs are dealt with once in the pleural space.

We examined the clearance of fibers from the pleural space by first showing the clearance of short radiola-

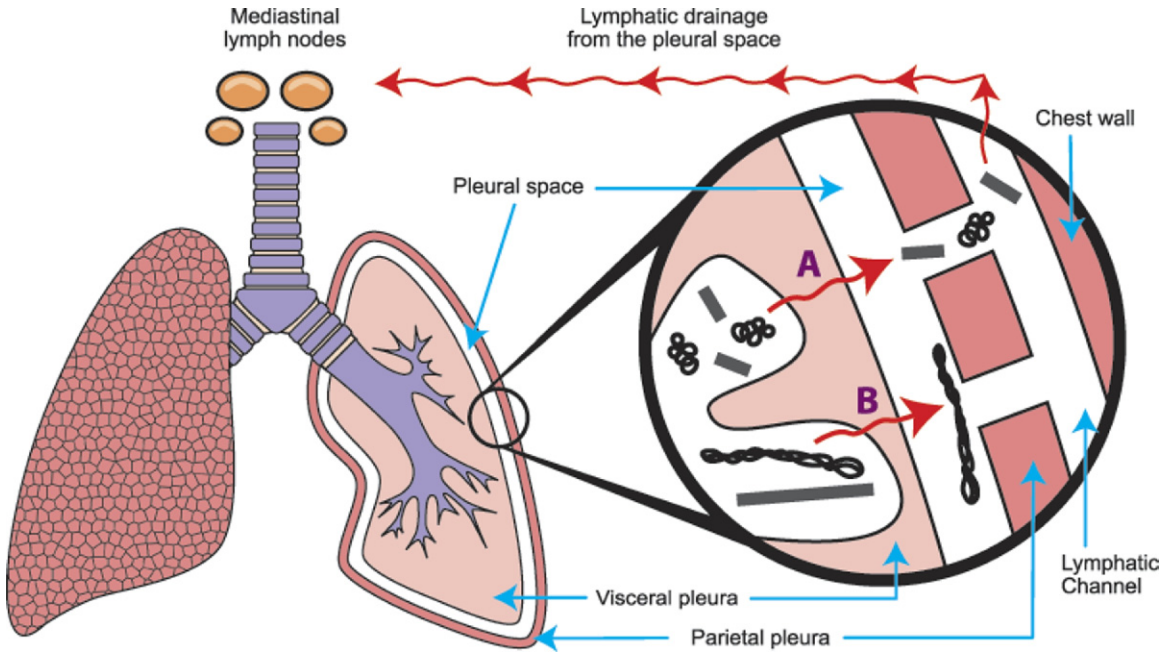

Figure 9. Diagrammatic representation of length-dependent clearance from the pleural space. **A:** Short fibers and small CNT tangles that deposit in alveoli that are situated subpleurally and migrate to the pleural space and exit in the flow of pleural fluid through the stomata, where they follow the lymphatic drainage to the mediastinal LNs. **B:** Long fibers and long CNTs also reach the pleural space from subpleural alveoli but they cannot negotiate the stomata and are retained, where they cause inflammation and potentially long-term disease.

beled CNTs instilled into the pleural space to the mediastinal LNs within 24 hours. Although a direct comparison of short and long CNTs would be ideal in this model, we could only use short CNTs because the process of radioactive labeling shortens long CNTs; therefore, we were unable to visualize, by this method, the retention of the long CNTs. However, this experiment allowed us to identify the cranial mediastinal LNs as the draining nodes for pleural drainage of particles. When we examined the fiber burden in these LNs after intrapleural injection of long and short CNTs, it was clear from the LN sections that the long CNT sample was not completely retained in the pleural space because of short fibers present in that sample that can translocate to the LNs. However, there was obviously more of the "short CNT" sample in the LNs than the "long CNT" sample. Although qualitative, this argues for retention of the longer fibers in the long CNT sample and translocation of the short fibers. We used the NiNWs that are present in tight-sized classes (ie, little short in the long and little long in the short) and demonstrated more convincingly that there was size-dependent retention because we saw only traces of nanowires in the LNs from animals exposed to long NiNWs but abundant nanowires in the LNs from animals that received intrapleural short NiNWs. The response in the LNs to the accumulations of short NiNWs was not closely examined; however, there were no changes in the gross morphological features or enlargement of the LNs of mice exposed to long or short CNTs or NiNWs when compared with vehicle control–treated mice.

We also saw a greater inflammatory response to the long NiNWs than the short NiNWs, strengthening the hypothesis that the pathogenicity of fibers in the pleural space is dependent on length rather than fiber composition. There have been suggestions that CNTs can undergo a degree of dissolution depending on their form[42,43]; thus, the retention/translocation kinetics of long CNTs from the pleural space could change over time if the CNTs undergo any biodissolution. Recently, Tomatis et al[44] reported that the greater toxicity of long asbestos fibers when compared with short asbestos fibers could be attributed to several factors other than length, including greater free radical production and reactive surface. Although these factors may give added toxicity to any fiber, we contend that the properties defined by the fiber pathogenicity paradigm (ie, length, thinness, and biopersistence) remain the primary attributes that a fiber must possess to elicit a pathogenic response. In particular, length will retain the harmful dose (eg, fiber-derived free radicals) in the pleural space; no matter how reactive any short fiber is, it will not remain in the pleural space to deliver its dose.[17] This theory was supported by the quartz and coal mine dust study (Figure 6). However, we are still not able to determine the size limit for retention in these studies. We believe that it should be possible to define a safe length below which there is no pleural retention, but we are unable to define this value based on the present experiments. It is a goal of future studies. However, for straight single fibers, such as NiNWs, our data show that the length beyond which there is parietal pleural retention is longer than approximately 4.3 μm, the length of the short NiNWs that were not retained; and $<\sim$24 μm, the length of the long NiNWs that were retained. Future studies will be aimed at refining this figure so that it more closely approaches the actual length limit.

In conclusion, we showed that injection of long nanofibers into the pleural space leads to persistent inflammation and eventually fibrosis at the parietal mesothe-

lium, where mesothelioma arises and other pleural pathological conditions may originate.[17] In contrast, short nanofibers cause no or modest resolving inflammation, with no parietal pleural pathological features (Figure 9). The data also support the contention that this length dependence is underlined by a dramatic difference in the retention of long fibers (versus short fibers) at stomata in the parietal pleura; the short fibers are cleared to the mediastinal LNs. These studies highlight the importance of fiber length in nanofiber toxicity to the pleura and illuminate the mechanism of the mesothelioma hazard from any long biopersistent fibers, such as asbestos, based on size-dependent retention and proinflammatory effects at the parietal pleura. This research illuminates our understanding of CNT toxicological features as they relate to fiber-type effects and suggests that any nanofiber that is aerodynamically small enough to enter the lungs satisfies the criteria of length and that biopersistence is likely to pose a similar hazard to the pleura. This is argued on the basis of the general relevance of a length-related mechanism of retention and the effect of biopersistence in enabling the long-fiber dose to be delivered to the mesothelium over a protracted time. The necessarily limited data on NiNW (a nanofiber of different composition from CNT) showed the predicted length-related inflammation in the pleural space. These and other data in preparation in our laboratory (not described herein), showing that silver nanowires also produce length-dependent inflammation in the pleural space, support the general relevance of the fiber pathogenicity paradigm for nanofibers. This has important public health implications for the likely risk that long biopersistent nanofibers might pose to the mesothelium if there is sufficient inhalation exposure and highlights the necessity for adequate risk assessment and management for people likely to be exposed to these fibers in workplace air.

Finally, although fiber length is clearly important for fiber effects in both the lung and pleural space, the understanding of the events in the pleural space described herein suggests that the critical length beyond which a long-fiber effect is induced might be different between the lungs and the pleura. In the lungs, the small aerodynamic diameter of fibers, provided that they are thin, means that long thin fibers easily reach the distal lung beyond the ciliated airways. In this position, the accumulation of the long-fiber dose is the result of frustrated phagocytosis and the failure of macrophages ingesting long fibers to make their way out of the lungs, with subsequent proinflammatory stimulation and genotoxicity in target cells. If fibers do reach the pleural space, the dominant feature dictating pathogenicity is retention at stomata because there is rapid clearance of all particles and fibers that are small enough to negotiate the parietal stomata. In the pleural space, much shorter fibers could be the source of problems than in the lungs because of the restricted anatomical "headroom" above the stomata caused by the close apposition of the visceral pleura. This would limit the ability of even short fibers to maneuver and negotiate the stomata and the convoluted subpleural lymphatic capillaries.

Acknowledgments

We thank Mitsui & Co and Dr. Ian Kinloch (University of Manchester, Manchester, UK) for the provision of MWCNT samples; and Stephen Mitchell (University of Edinburgh, Edinburgh, UK) for sample preparation for SEM and technical assistance.

References

1. Donaldson K, Aitken R, Tran L, Stone V, Duffin R, Forrest G, Alexander A: Carbon nanotubes: a review of their properties in relation to pulmonary toxicology and workplace safety. Toxicol Sci 2006, 92:5–22
2. Maynard AD: Nanotechnology: the next big thing, or much ado about nothing? Ann Occup Hyg 2007, 51:1–12
3. Maynard AD, Aitken RJ, Butz T, Colvin V, Donaldson K, Oberdorster G, Philbert MA, Ryan J, Seaton A, Stone V, Tinkle SS, Tran L, Walker NJ, Warheit DB: Safe handling of nanotechnology. Nature 2006, 444:267–269
4. Shvedova AA, Kisin ER, Porter D, Schulte P, Kagan VE, Fadeel B, Castranova V: Mechanisms of pulmonary toxicity and medical applications of carbon nanotubes: two faces of Janus? Pharmacol Ther 2009, 121:192–204
5. Kostarelos K: The long and short of carbon nanotube toxicity. Nature Biotechnol 2008, 26:774–776
6. Mossman BT, Churg A: Mechanisms in the pathogenesis of asbestosis and silicosis. Am J Respir Crit Care Med 1998, 157:1666–1680
7. Donaldson K, Tran CL: An introduction to the short-term toxicology of respirable industrial fibres. Mutat Res 2004, 553:5–9
8. Craighead JE, Abraham JL, Churg A, Green FH, Kleinerman J, Pratt PC, Seemayer TA, Vallyathan V, Weill H: The pathology of asbestos-associated diseases of the lungs and pleural cavities: diagnostic criteria and proposed grading schema: report of the Pneumoconiosis Committee of the College of American Pathologists and the National Institute for Occupational Safety and Health. Arch Pathol Lab Med 1982, 106:544–596
9. Davis JG, Addison J, Bolton RE, Donaldson K, Jones AD, Smith T: The pathogenicity of long versus short fiber samples of amosite asbestos administered to rats by inhalation and intraperitoneal injection. Br J Exp Pathol 1986, 67:415–430
10. Kane AB. Mechanisms of mineral fibre carcinogenesis. Mechanisms of Fibre Carcinogenesis. Edited by AB Kane, P Boffetta, R Saracci, JD Wilbourn. IARC Sci Pub 1996, pp 11–34
11. Poland CA, Duffin R, Kinloch I, Maynard A, Wallace WA, Seaton A, Stone V, Brown S, MacNee W, Donaldson K: Carbon nanotubes introduced into the abdominal cavity of mice show asbestos-like pathogenicity in a pilot study. Nat Nanotechnol 2008, 3:423–428
12. Kane AB, Macdonald JL, Moalli PA: Acute injury and regeneration of mesothelial cells produced by crocidolite asbestos fibers. Am Rev Respir Dis 1986, 133:A198
13. Wagner JC, Pooley FD: Mineral fibers and mesothelioma. Thorax 1986, 41:161–166
14. Wang NS: The preformed stomas connecting the pleural cavity and the lymphatics in the parietal pleura. Am Rev Respir Dis 1975, 111:12–20
15. Mitchev K, Dumortier P, De Vuyst P: "Black spots" and hyaline pleural plaques on the parietal pleura of 150 urban necropsy cases. Am J Surg Pathol 2002, 26:1198–1206
16. Muller KM, Schmitz I, Konstantinidis K: Black spots of the parietal pleura: morphology and formal pathogenesis. Respiration 2002, 69:261–267
17. Donaldson K, Murphy FA, Duffin R, Poland CA: Asbestos, carbon nanotubes and the pleural mesothelium: a review of the hypothesis regarding the role of long fibre retention in the parietal pleura, inflammation and mesothelioma. Part Fibre Toxicol 2010, 7:5
18. Byrne F, Prina-Mello A, Whelan A, Mohamed BM, Davies A, Gun'ko YK, Coey JMD, Volkov Y: High content analysis of the biocompatibility of nickel nanowires. J Magn Magn Mater 2009, 321:1341–1345
19. Prina-Mello A, Diao Z, Coey J: Internalization of ferromagnetic nanowires by different living cells. J Nanobiotechnol 2006, 4:9
20. Shinohara H: Distribution of lymphatic stomata on the pleural surface of the thoracic cavity and the surface topography of the pleural mesothelium in the golden hamster. Anat Rec 1997, 249:16–23

21. Li SP, Wu W, Campidelli S, Sarnatskaia V, Prato M, Tridon A, Nikolaev A, Nikolaev V, Bianco A, Snezhkova E: Adsorption of carbon nanotubes on active carbon microparticles. Carbon 2008, 46:1091–1095
22. Wright G, Kuschner M. The influence of varying lengths of glass and asbestos fibers on tissue responses in the guinea pigs. Inhaled Particles, vol 4. Edited by WH Walton. Oxford, Pergamon Press, 1977, pp 455–474
23. Drew RT, Kuschner M, Bernstein DM: The chronic effects of exposure of rats to sized glass fibres. Ann Occup Hyg 1987, 31:711–729
24. Donaldson K, Brown GM, Brown DM, Bolton RE, Davis JM: Inflammation generating potential of long and short fibre amosite asbestos samples. Br J Ind Med 1989, 46:271–276
25. Goodglick LA, Kane AB: Cytotoxicity of long and short crocidolite asbestos fibers in vitro and in vivo. Cancer Res 1990, 50:5153–5163
26. Ye J, Shi X, Jones W, Rojanasakul Y, Cheng N, Schwegler-Berry D, Baron P, Deye GJ, Li C, Castranova V: Critical role of glass fiber length in TNF-alpha production and transcription factor activation in macrophages. Am J Physiol 1999, 276(Pt 1):L426–L434
27. Dogra S, Donaldson K: Effect of long and short fibre amosite asbestos on in vitro TNF production by rat alveolar macrophages: the modifying effect of lipopolysaccharide. Ind Health 1995, 33:131–141
28. Brown DM, Kinloch IA, Bangert U, Windle AH, Walter DM, Walker GS, Scotchford CA, Donaldson K, Stone V: An in vitro study of the potential of carbon nanotubes and nanofibres to induce inflammatory mediators and frustrated phagocytosis. Carbon 2007, 45:1743–1756
29. Boutin C, Rey F, Gouvernet J, Viallat JR, Astoul P, Ledoray V: Thoracoscopy in pleural malignant mesothelioma: a prospective study of 188 consecutive patients: part 2: prognosis and staging. Cancer 1993, 72:394–404
30. Moalli PA, Macdonald JL, Goodglick LA, Kane AB: Acute injury and regeneration of the mesothelium in response to asbestos fibers. Am J Pathol 1987, 128:426–445
31. Vasilieva LA, Pylev LN, Rovensky YA: Pathogenesis of experimentally induced asbestos mesothelioma in rats. Cancer Lett 1998, 134:209–216
32. Bernstein DM, Rogers RA, Sepulveda R, Donaldson K, Schuler D, Gaering S, Kunzendorf P, Chevalier J, Holm SE: The pathological response and fate in the lung and pleura of chrysotile in combination with fine particles compared to amosite asbestos following short-term inhalation exposure: interim results. Inhal Toxicol 2010, 22:937–962
33. Kanazawa K, Roe FJ, Yamamoto T: Milky spots (Taches-laiteuses) as structures which trap asbestos in mesothelial layers and their significance in the pathogenesis of mesothelial neoplasia. Int J Cancer 1979, 23:858–865
34. Roberts GH: The pathology of parietal pleural plaques. J Clin Pathol 1971, 24:348–353
35. Brown GM, Donaldson K: Inflammatory responses in lungs of rats inhaling coal-mine dust: enhanced proteolysis of fibronectin by bronchoalveolar leukocytes. Br J Ind Med 1989, 46:866–872
36. Donaldson K, Brown GM, Brown DM, Robertson MD, Slight J, Cowie H, Jones AD, Bolton RE, Davis JM: Contrasting bronchoalveolar leukocyte responses in rats inhaling coal mine dust, quartz, or titanium dioxide: effects of coal rank, airborne mass concentration, and cessation of exposure. Environ Res 1990, 52:62–76
37. Lapp NL, Castranova V: How silicosis and coal workers' pneumoconiosis develop: a cellular assessment. Occup Med 1993, 8:35–56
38. Parungo CP, Colson YL, Kim SW, Kim S, Cohn LH, Bawendi MG, Frangioni JV: Sentinel lymph node mapping of the pleural space. Chest 2005, 127:1799–1804
39. Ryman-Rasmussen JP, Cesta MF, Brody AR, Shipley-Phillips JK, Everitt JI, Tewksbury EW, Moss OR, Wong BA, Dodd DE, Andersen ME, Bonner JC: Inhaled carbon nanotubes reach the subpleural tissue in mice. Nat Nanotechnol 2009, 4:747–751
40. Mercer RR, Hubbs AF, Scabilloni JF, Wang LY, Battelli LA, Schwegler-Berry D, Castranova V, Porter DW: Distribution and persistence of pleural penetrations by multi-walled carbon nanotubes. Part Fibre Toxicol 2010, 7:28
41. Miserocchi G, Sancini G, Mantegazza F, Chiappino G: Translocation pathways for inhaled asbestos fibers. Environ Health 2008, 7:4
42. Liu XY, Hurt RH, Kane AB: Biodurability of single-walled carbon nanotubes depends on surface functionalization. Carbon 2010, 48: 1961–1969
43. Kagan VE, Konduru NV, Feng W, Allen BL, Conroy J, Volkov Y, Vlasova II, Belikova NA, Yanamala N, Kapralov A, Tyurina YY, Shi J, Kisin ER, Murray AR, Franks J, Stolz D, Gou P, Klein-Seetharaman J, Fadeel B, Star A, Shvedova AA: Carbon nanotubes degraded by neutrophil myeloperoxidase induce less pulmonary inflammation. Nat Nanotechnol 2010, 5:354–359
44. Tomatis M, Turci F, Ceschino R, Riganti C, Gazzano E, Martra G, Ghigo D, Fubini B: High aspect ratio materials: role of surface chemistry vs length in the historical "long and short amosite asbestos fibers." Inhalation Toxicol 2010, 22:984–998